IPEM-Translation 1 (2022) 100003

Contents lists available at ScienceDirect

IPEM-Translation

journal homepage: www.elsevier.com/locate/ipemt

Full Length Article

Finite Element Analysis of Identifying Breast Cancer Tumor Grades Through Frequency Spectral Variation of High-Frequency Ultrasound

Koushik Paul[a,*], Jeremy Stromer[b], Samuel Razmi[c], Barbara A. Pockaj[d], Leila Ladani[e]

[a] School for Engineering of Matter, Transport and Energy, Ira A. Fulton Schools of Engineering, Arizona State University, Tempe, AZ 85281, USA
[b] Survivability Engineering Branch, US Army Engineer Research and Development Center, Vicksburg, MS 39180, USA
[c] EnMed Department, Texas A&M College of Medicine, Houston, TX 77807, USA
[d] Mayo Clinic in Arizona, Surgery, Phoenix, AZ 85054, USA
[e] School for Engineering of Matter, Transport and Energy, Ira A. Fulton Schools of Engineering, Arizona State University, Tempe, AZ 85281, USA

ARTICLE INFO

Keywords:
Histology-based modeling
acoustic scattering
peak density
high-frequency ultrasound
tumor grading
breast cancer
mitotic rate
pleomorphism

ABSTRACT

Ultrasound analysis is an instantaneous characterization tool to evaluate microstructural inhomogeneity. In this study, computational high-frequency ultrasound analysis was conducted to characterize histological features of malignant breast tissue. A high-frequency ultrasound signal was sent through the soft tissue model in a through-transmission manner. Histological features of the soft tissue were categorized as cell shape, nuclear pleomorphism, and malignant cell density. The design of experiment was created by combining various levels of histological features of tumor tissue. Transmitted ultrasound frequency spectrums from all combinations of histological features were analyzed in terms of peak density and mean peak to valley distance (MPVD) parameters. For the circular-shaped cell model, peak density and MPVD responded with increasing and decreasing trends respectively while the malignant histological features became gradually dominant. For the elliptical-shaped cell model, only peak density was effective to establish a relationship with the histological features. It was observed that added malignant cells had more contribution to the response parameters than nuclear pleomorphism. Furthermore, the frequency spectrum patterns from all histological combinations were evaluated to find further information about malignant features.

Introduction

Breast cancer which is also known as breast carcinoma is an uncontrolled growth of epithelial cells in the breast [1]. It is the second most common cancer in women but can affect men as well [2]. Each time cells divide inside breast ducts or lobules there is a chance of genetic mutation causing uncontrolled growth of cells resulting in tumor formation [1]. To develop a characterization method for identifying the malignancy/cancer, computational modeling can be an important tool to understand the cellular level behavior under an external characterization system [3,4]. To model the breast tumor, it is very important to know the difference between the tumor tissue and normal tissue. It is understood that the presence of abnormally high-dense tissue in the breast lobule may be a good indicator of a tumor [5]. This higher density normally occurs through an increasing percentage of the fibro glandular tissue in the breast [6,7]. Pathologists use a grading system to specify the aggressiveness of tumor cells. The grading system consists of three factors: (1) percentage of cancer cells formed into tubules, (2) difference in the nuclei size between healthy and malignant cells (nuclear pleomorphism), and (3) rate of cancerous cell division [8,9]. Based on these factors, pathologists divide the tumor into three grades where the higher the grade, the larger the difference in histological structures between cancerous and normal tissue.

Different types of analysis were conducted to investigate the relationship between histological features and ultrasound parameters. Empirical analysis showed a strong correlation between histological changes in properly characterized tissues and ultrasound scattering [10,11]. In the case of experimental outcomes, empirical models were only relevant for homogenous tissues [12]. For the analytical analysis, ultrasound scattering was averaged from the uniform distribution of cells which simplified the acoustic scattering [13]. Therefore, the effect of structural heterogeneity, wave-mode conversion, and multiple scattering was ignored in analytical analysis. To overcome these issues, the iterative multipole simulation method was utilized to accurately evaluate the ultrasound analysis parameters to detect the changes in histological features [14,15]. In these studies, histological features like the size of the cell and nucleus were evaluated. These simulation models successfully evaluated multiple ultrasonic scattering in complex

* Corresponding Author
E-mail addresses: kpaul5@asu.edu (K. Paul), jeremy.d.stromer@erdc.dren.mil (J. Stromer), samrazmi@tamu.edu (S. Razmi), pockaj.barbara@mayo.edu (B.A. Pockaj), leila.j.ladani@gmail.com (L. Ladani).

https://doi.org/10.1016/j.ipemt.2022.100003
Received 28 November 2021; Received in revised form 8 March 2022; Accepted 24 March 2022
Available online 25 March 2022

histological structures while taking wave mode propagation into account. But the studies did not include viscoelasticity, and the cellular shape could have been more histologically accurate. The multiple scattering was also limited to a range of cells. Furthermore, the transducer properties could also be closely approximated in the numerical models.

Backscattered ultrasound measurements were mostly evaluated in the above-mentioned studies [13,15–17]. Compared to the backscattered ultrasound, in the forward scattering measurement, the ultrasound wave has to travel half of the distance. In that case, the wave gets less attenuated. Therefore, the scattered quantitative ultrasound spectrum is more pronounced with details. The potential of the forward scattering for histology-based evaluation is yet to be explored. In the case of evaluating backward scattering, the pulse-echo mode of ultrasound analysis was used wherein the case of the forward scattering, pitch-catch, or through transmission ultrasound analysis mode was applied [18,19]. In this research, the later mode was used to evaluate different spectral parameters from the forward scattering. During ultrasound propagation through the medium, acoustic scattering is a very important factor controlling the response parameters. When the acoustic wave collides with another medium with different sound velocities, it scatters in different directions depending on the wavelength and medium structure size [20]. Based on the number of structures on the acoustic propagation path, there could be either single or multiple acoustic scattering [15,21]. At the microscopic histological level, multiple scattering occurs at two different levels. Firstly, the scattered wave from numerous cells causes one level of multiple scattering. Secondly, scattered waves from the different intra-cellular interfaces (ECM-cytoplasm, and cytoplasm-nucleus) inside a cell can cause another level of multiple scattering [15]. Based on the frequency range, acoustic wave scattering can also be categorized into different levels [22]. In the case of breast tissue, multiple scattering was found very significant for the frequencies at approximately 4 MHz [23]. In that frequency level, diffuse ultrasound scattering occurs where the scattered wave goes in all directions with equal magnitude. But at the high-frequency level, diffractive scattering occurs where wave scatters in all directions with different amplitude [18]. It was found that in diffractive scattering, the ultrasound response parameters were strongly dependent on structure size, numbers, and propagation path [20,24].

The goal of this study was to identify various histological features of the tumor tissue through high-frequency ultrasound (22-41 MHz). Compared to the experimental ultrasound measurement, computational analysis enables us to understand the acoustic-cell interaction at the microscopic level and utilize it to explain the results from ultrasound analysis. Therefore, high-frequency ultrasound analysis was conducted computationally to evaluate multiple forward acoustic scattering to detect different histological features of cancerous tissue. Two important factors from the histological grading were considered for the design of experiment (DOE) of tissue modeling which was nuclear pleomorphism and malignant cell density. By increasing the level of these factors in the DOE, the increasing malignancy level in the tumor tissue was depicted. The DOE also included two different cellular shapes- circular for initial approximation and elliptical for a close approximation. 22 to 41 MHz frequency range was used in this study to keep similarity with the previous research [20,25]. Different response parameters in the frequency domain were evaluated in this study. One of the response parameters was spectral peak density that was found very responsive against microstructural changes [25,26] The average magnitude difference between all the adjacent peaks and valleys was also analyzed which was called Mean Peak to Valley Distance (MPVD). Furthermore, the spectral pattern was analyzed to find out significant features of the spectrum from various malignant features. It was observed that with cellular structures tending towards the cancerous level, peak density increased and MPVD value decreased. Also, the malignant cell density contributed more to the multiple scattering than the pleomorphism.

Design of experiment

In the case of nuclear pleomorphism, a total of 4 levels of nuclear diameter were used. The nuclear diameter of the healthy cell was kept as 10 μm. To delineate the gradual severity of the cancerous stage, the nuclear diameter was increased by 20% (12 μm), 40% (14 μm), and 60% (16 μm) in the tumor tissue model. For the initial stage, the number of healthy epithelial cells was kept as 750. In the case of increasing malignant cell density, the number of added malignant cells in normal tissue was 375 and 750. Therefore, with increasing cellular density, the total number of cells became 1125, and 1500 respectively. Furthermore, in previous research, the cells were approximated as spherical shaped where it was found that a closer approximation could be achieved through spheroidal cellular shape [15]. Therefore, the cellular shape was also considered as another factor for the DOE. Since simulations were conducted in two-dimensional models, the spherical and spheroidal cellular shapes were considered circular and elliptical, respectively. Another approximation was considered that the cell cross-sections were all taken from their center plane. Thus, the area of the cell and nucleus was kept uniform in all DOE combinations. Furthermore, to model elliptical cells, the direction of the major and minor axis of the ellipse became an important factor to consider. Since, in the cancerous stage, the malignant cells were arranged loosely from each other, the elliptical cells' major and minor axis could be in any direction inside the tissue. In this study, only two orientations of the elliptical cells were considered (horizontal and vertical). These orientations were equally distributed between normal and malignant cells.

In summary, the DOE consisted of 3 factors where the factors- nuclear pleomorphism, malignant cell density, and cellular shape consisted of 4, 2, and 2 levels, respectively. Therefore, a total of 24 combinations were created for the computational analysis.

Table 1 shows all the combinations that were analyzed in this study. From this table, combination 1 depicted the healthy breast tissue, and combination 2 and 14 only showed increased cell density with no pleomorphism. Thus, combinations 2 and 14 were depicted as dense breast tissues with no malignancy. Combinations 4, 7, and 10 from the circular shape model were similar to combination 1. Combinations 16, 19, and 22 from the elliptical cell model were similar to combination 13. In both cases, since there were no added malignant cells, nuclear pleomorphism was not considered. But these combinations were kept in this table to maintain consistency of the DOE.

For characterizing these different combinations, two response parameters were analyzed in this study. One of the response parameters was the ultrasound peak density of the frequency spectrum. As the name suggests, peak density is the total amount of peaks and valleys in the frequency domain spectrum of the transmitted ultrasound signal (pitch-catch mode). The second response parameter was Mean Peak to Valley Distance (MPVD). MPVD parameter was simply calculated from the frequency spectrum by calculating the average value of all the adjacent peak to valley distances [22]. Furthermore, the spectral pattern (large peaks or valleys, jaggedness, etc.) was analyzed to extract detailed frequency information for evaluating tissue microstructure at different malignancy levels.

Model description

In the model geometry, the cells were generated randomly for both normal and malignant cases. Thus, the model depicted loosely bonded cells inside the tissue. The model consisted of extracellular matrix, cytoplasm, and nucleus. Fig. 1 depicts the model geometry for combinations 12 and 24 from the DOE. Both combinations had normal cells as well as malignant cells where the cellular shape was circular and elliptical, respectively. The malignant cells were evident in the model geometry as they had a larger nucleus (60% pleomorphism). In the case of the elliptical geometry, the cells were arranged in two different orientations based on their major and minor axis. An ultrasound plane wave was

Table 1
Design of experiment (DOE)

Comb. no.	Cell shape	Increase in malignant nucleus diameter (%)	Added number of malignant cells	Comb. no.	Cell shape	Increase in malignant nucleus diameter (%)	Added number of malignant cells
1	Circular	0	0	13	Elliptical	0	0
2	Circular	0	375	14	Elliptical	0	375
3	Circular	0	750	15	Elliptical	0	750
4	Circular	20	0	16	Elliptical	20	0
5	Circular	20	375	17	Elliptical	20	375
6	Circular	20	750	18	Elliptical	20	375
7	Circular	40	0	19	Elliptical	40	0
8	Circular	40	375	20	Elliptical	40	375
9	Circular	40	750	21	Elliptical	40	750
10	Circular	60	0	22	Elliptical	60	0
11	Circular	60	375	23	Elliptical	60	375
12	Circular	60	750	24	Elliptical	60	750

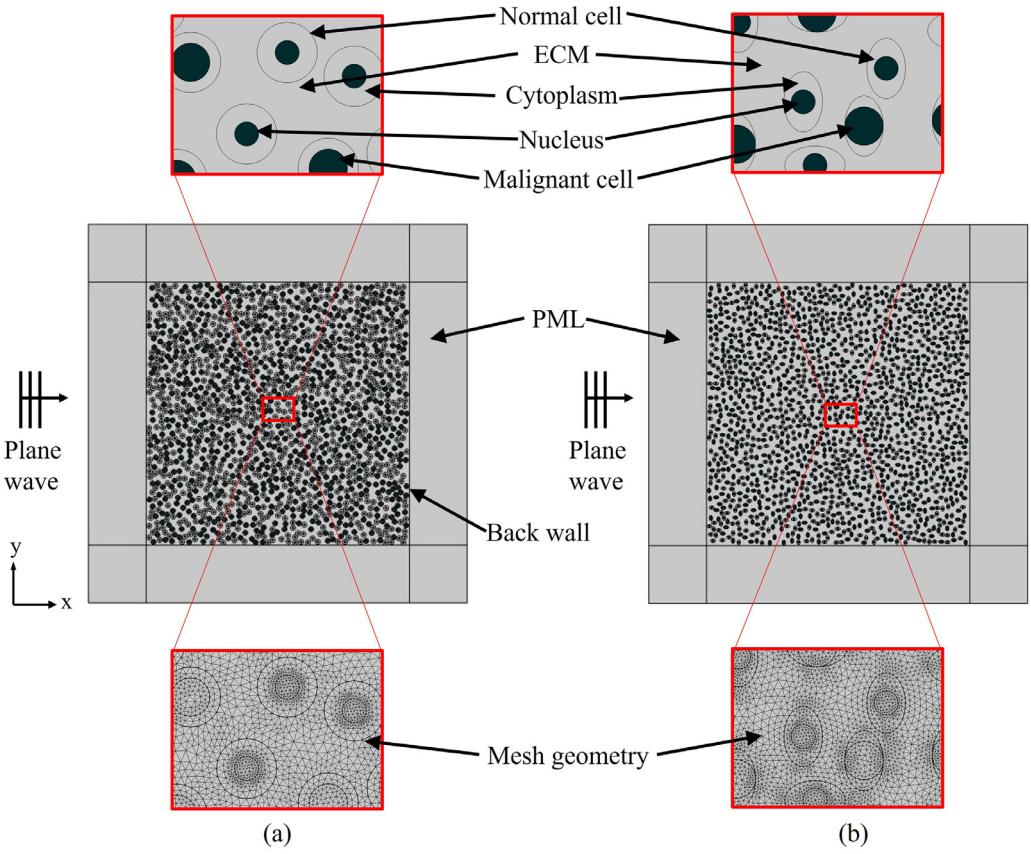

Fig. 1. Model geometry of (a) combination 12 and (b) combination 24 from the DOE

sent in the positive x-direction. For smooth acoustic wave propagation through the tissue boundary, a perfectly matched layer (PML) was introduced in the model. The 2D model area was 1300 μm x 1300 μm in dimension. In the case of the circular-shaped cellular model, the cell diameter was 25 μm [27,28]. For the elliptical-shaped cellular model, the major and minor axis lengths of the cell were approximated 25 μm and 16 μm respectively.

Simulation physics

Previously, computational modeling was conducted by approximating the ECM, nucleus, and cytoplasm as both solid and fluid [15]. Since the goal of this research was to explore the multiple scattering and different geometric features of the cell, all histological features were considered fluid. COMSOL Multiphysics v5.6 software was used to conduct all the simulations. In the fluid medium, the acoustic wave propagation follows the Helmholtz equation shown in Eq. (1). The equation provides the acoustic pressure distribution as a function of frequency inside the medium.

$$\nabla.\left(-\frac{1}{\rho_c}\left(\nabla p_t - \boldsymbol{q_d}\right)\right) - \frac{k_{eq}^2}{\rho_c} p_t = Q_m \tag{1}$$

In fluid, for the speed of sound c_c, attenuation coefficient α, and frequency f, the equivalent wave number, k_{eq} can be shown as

$$k_{eq}^2 = \left(\frac{2\pi f}{c_c} - i\ln(10)\frac{\alpha}{20}\right)^2 - k_z^2 = k^2 - k_z^2 \tag{2}$$

Table 2
Material properties

	ECM	Cytoplasm	Nucleus
Density, $\rho_c (kgm^{-3})$	1060	998	1430
Longitudinal wave speed, $c_c (ms^{-1})$	1570	1483	1509
Attenuation coefficient, $\alpha (dBm^{-1}MHz^{-1})$	70	70	70

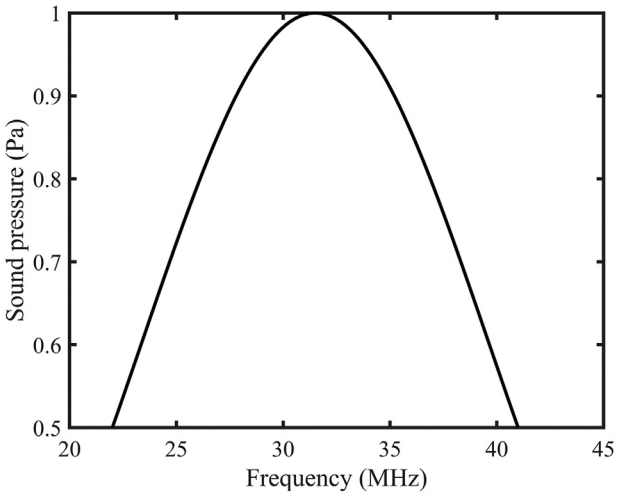

Fig. 2. Background pressure distribution over the input frequency range

In this model, out of plane wave number k_z is set to zero. Monopole and dipole source term Q_m and $\boldsymbol{q_d}$ are both zero in this system. ρ_c is the fluid density. The total pressure, p_t is the summation of the background pressure field (p_b) and scattered pressure field (p_s). In the model, the background pressure field is expressed as wave propagation in $\hat{e_x}$ direction defined as $p_b = p_0 e^{-ikx}$. Here k is the wavenumber which is the function of frequency (f) shown in Eq. (2).

Material properties in ECM, cytoplasm, and nucleus are included in Table 2 [29,30].

The simulation was conducted for a high-frequency range from 22 to 41 MHz mimicking a high-frequency transducer with frequency bandwidth. In general, ultrasound transducers send pressure waves for a frequency range where the pressure magnitude is distributed as a bell-shaped curve and the maximum pressure magnitude is found at the center frequency. Therefore, the input background pressure for this model was distributed in a bell-shaped pattern over the frequency range and the maximum pressure amplitude was kept at 31.5 MHz (Fig. 2). Furthermore, the frequency bandwidth was selected at 50% of the maximum amplitude. Therefore, pressure at 31.5 MHz was selected as 1 Pa and at both 22 and 41 MHz, it was kept 0.5 Pa (50% of max amplitude).

The frequency step size was 100 kHz for this model. Therefore, from the 22 to 41 MHz range, the model calculated scattered pressure for 190 frequency points. To mimic the pitch-catch method, the average scattered pressure for each frequency point was measured from the back wall of the model geometry shown in Fig. 1. Then the frequency spectrum was generated by accumulating all the scattered pressure in the frequency range. The free triangular mesh was used in the tissue geometry and the mapped mesh was used in the PML region. Mesh element size was selected as one-sixth of the wavelength.

To calculate the peak density, the number of peaks and valleys were counted from the frequency spectrum [17]. For calculating the MPVD parameter, the average pressure difference between all adjacent peaks and valleys was measured.

Results

Fig. 3 represents the peak density data from all the histological feature combinations in the cellular cell and elliptical cell model. In both models, it was evident that the peak density followed an overall increasing pattern with the increased number of malignant cells as well as increased nucleus size (pleomorphism). In the circular cell model (Fig. 3a), the trend was more evident compared to the elliptical cell model (Fig. 3b). The possible reason behind that could be the uniform cell area surrounding the nucleus in the circular model. This uniform cell shape created a homogeneous intra-cellular scattering compared to the elliptical cell model.

In the case of the MPVD result, an overall decreasing trend with increasing histological features (cell density, pleomorphism) was observed only for the circular cell model (Fig. 4a). The elliptical cell model failed to create a general correlation between MPVD and the histological features (Fig. 4b).

The spectral patterns were also analyzed in this research to extract further information about different malignancy levels. For both cellular and elliptical models, the frequency spectrums were divided into two groups. Group 1 consisted of the signals acquired from 375 added malignant cells (Fig. 5a and Fig. 6a), and group 2 consisted of the signals acquired from 750 added malignant cells (Fig. 5b and Fig. 6b). In both groups, the frequency spectrum from normal/healthy tissue (without malignant cells and pleomorphism) was added as a reference to visualize the change in spectrums for different malignant grades. In the case of the circular cell model, from Fig. 5a, it was evident that all the spectrums with 375 malignant cells followed the overall bell-shaped pattern of the input background pressure. For the healthy tissue spectrum, a large peak between 30 to 35 MHz region was observed. The pressure magnitude differences between that peak to its adjacent valleys were approximately 1 Pa. A similar peak with a slightly increased pressure magnitude of 1.06 Pa was seen when 375 cells were added with no pleomorphism (dense healthy tissue). But with increasing nuclear pleomorphism in the 375 malignant cells, the peak started to disappear. And finally, with 60% pleomorphism, the peak completely disappeared from the malignant tissue spectrum. In the case of the 750 added malignant cells (Fig. 5b), this pattern was more pronounced. In the case of 750 added cells, for the dense healthy tissue, the peak between 30-35 MHz region had a much higher amplitude than the healthy tissue spectrum. Although it was not a smooth peak, the envelope of the spectrum in that region depicted a peak with a pressure magnitude of 1.65 Pa. But the peak started to vanish and showed random spectrum jaggedness with increased nucleus size. Finally, similar to the 375 malignant cells, the peak completely vanished with 60% increased nucleus size in malignant tissue. Overall, in both 375 and 750 malignant cells, the jaggedness (fluctuation in the pressure magnitude) in the frequency spectrum started to increase with increasing nucleus size.

In the case of the elliptical cell shown in Fig. 6, the spectrums with 375 and 750 cells followed an overall similar pattern to the circular cell. One major difference compared to the circular model was that there were two distinguished peaks (0.4 Pa and 0.3 Pa) instead of one in the healthy tissue spectrum. Similar to the circular model, the peak magnitude for the dense healthy tissue (375 cells) increased (0.95 Pa and 0.45 Pa). But in the case of dense healthy tissue with 750 additional normal cells, the peaks merged into one with an increasing magnitude of 0.8 Pa. The peaks were still visible in the case of low pleomorphism (20%) but the jaggedness started to become visible. Then similar to the circular cell model, these peaks gradually disappeared with increased pleomorphism, and irregular jaggedness was observed in their pattern. Another difference that was spotted in the elliptical cell spectrums was the overall scattered pressure amplitude. All the spectrums with added malignant cells had a higher amplitude level compared to the healthy tissue spectrum.

From the spectral pattern, it was observed that although the nuclear pleomorphism had less of an effect on the response parameters (peak

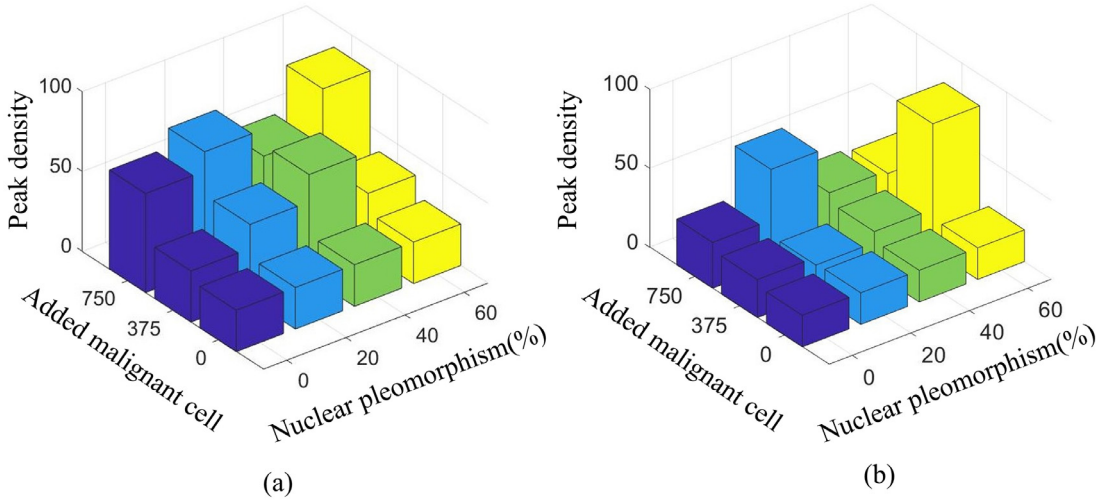

Fig. 3. Peak density for (a) circular cell model, (b) elliptical cell model

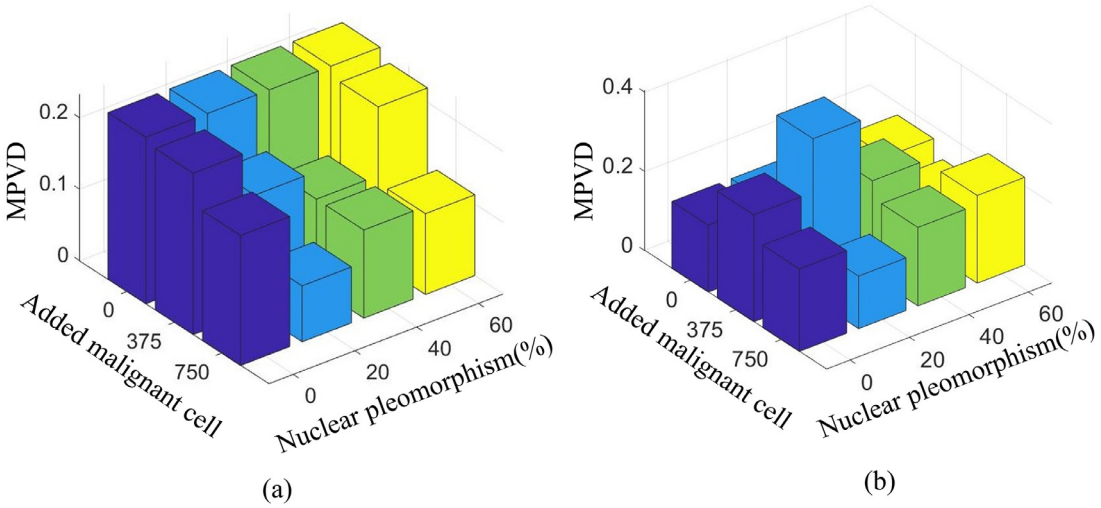

Fig. 4. MPVD for (a) circular cell model, (b) elliptical cell model

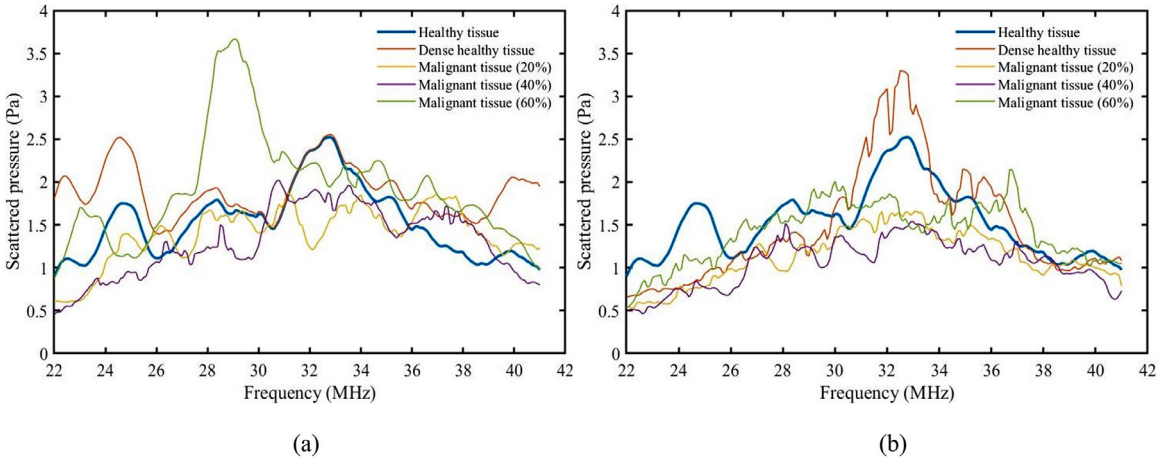

Fig. 5. Circular cell: frequency spectrum of the normal histological spectrum with (a) spectrums for 375 added malignant cells at all pleomorphism levels, (b) spectrums for 750 added malignant cells at all pleomorphism levels

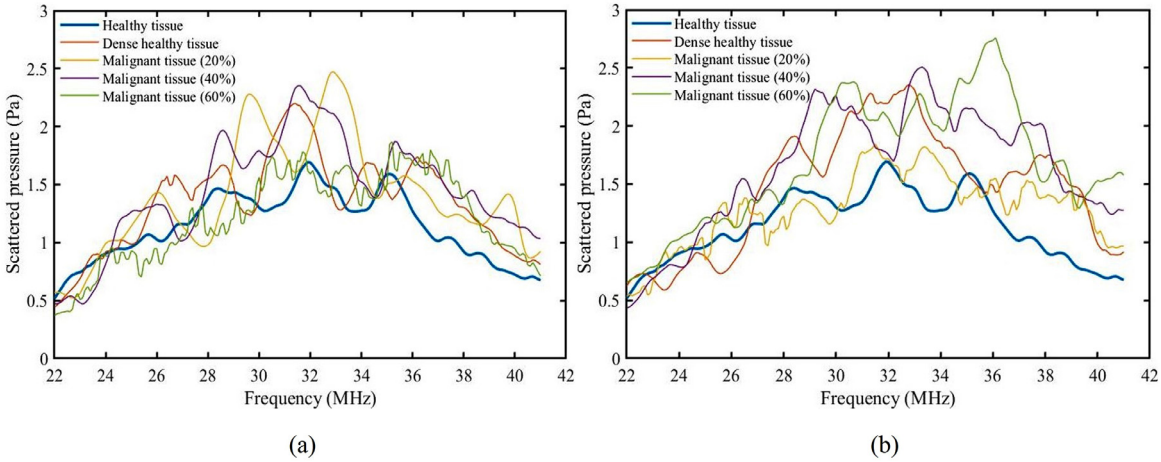

Fig. 6. Elliptical cell: frequency spectrum of the normal histological spectrum with (a) spectrums for 375 added malignant cells at all pleomorphism levels, (b) spectrums for 750 added malignant cells at all pleomorphism levels

density and MPVD), it certainly affected the frequency spectrum. Therefore, by studying the frequency spectrum, information about nuclear pleomorphism can be extracted.

Discussion

While using quantitative ultrasound parameters to characterize tumor microstructure, it was found that peak density was a more effective parameter than MPVD. In Fig. 3, it was observed that for both circular and elliptical cell models, the increase in peak density was more evident in the "added malignant cell" axis. Added malignant cell or increasing malignant cell density in this study was nothing but an increasing number of scatterers. The QUS parameter peak density is dependent on the amount of multiple acoustic scattering that occurs inside the tissue microstructure. From a previous study, it was found that multiple scattering occurring from the added number of scatters had a major effect on peak density [20]. Therefore, this trend of peak density data made perfect sense in this case. Also, it was understood that the aggressiveness of tumors in terms of the mitotic rate will be more identifiable through peak density data.

In terms of the MPVD data, a decreasing trend was observed with increasing histological feature levels. MPVD variation depends on the peak to valley pressure difference in the frequency spectrum. Therefore, if the spectrum patterns remain similar while the peak to valley pressure magnitude varies, the MPVD trend could be more conclusive. In this study, since the cells were randomly dispersed, the scattering behavior was fully random. Even though the spectrums in all cases had a similarity at a certain level, the pressure magnitude was too random to provide a meaningful MPVD pattern. In the case of the circular cell, the scattered wavefront from the cells was consistent in all directions compared to the elliptical cells because of their geometry. In the horizontal elliptical cell, the forward scattering was more dominant compared to the vertical elliptical cell. Therefore, the randomness in scattering from the elliptical cell was more prominent compared to the circular cell. This scattering randomness might be optimized, and the computational model would be more realistic if the elliptical cell orientation was random instead of only being horizontal and vertical. The only time MPVD showed a consistent decreasing trend, was for the added malignant cell parameter in the circular cell model. Although having random cell distribution, the shape consistency helped to create a better MPVD response in that case. It indicated that with increased scattering due to excess malignant cells, the peak to valley pressure magnitude decreased over the frequency bandwidth. Overall, for random cell dispersion, MPVD was not an effective response parameter to analyze. Thus, it can be said that while using quantitative ultrasound for tumor grading, the cellular shape will also be the key factor.

To reinforce the peak density results, the spectral comparison was conducted in this study. Spectral features like center frequency pressure magnitude (center peak) could be a supporting indicator of whether the malignancy has started to occur inside the tissue sample. It was more of a qualitative measurement rather than a quantitative measurement. The authors could not perform a quantitative analysis of the spectral comparison because of the randomness of the spectral shape of the malignant tumor in the center frequency region.

In a previous study, it was found that among different quantitative ultrasound parameters, peak density was comparatively more sensitive towards the material microstructure [31]. This study showed the feasibility of quantitative ultrasound peak density in detecting tissue microstructure through the evaluation of acoustic-cell interactions. A relevant application of this method can be intraoperative surgical margin analysis during breast conservation surgery [32]. Labor intensive post-operative margin tissue analysis increases the reoperation rate as well as local recurrence rate [33–35]. Developing an ultrasound device based on this study can instantaneously provide information regarding the presence of malignant cells inside margin tissue. This information will help the surgeons to take the necessary decisions to proceed with further excisions during the first surgery. In addition to characterizing the breast tumor, this method can be utilized in various diagnostic applications where the cellular microstructure needs to be analyzed. In terms of cancer detection, this method can be implemented for prostate cancer detection, metastasis detection in lymph node tissues, differentiating between melanoma and non-melanoma skin cancers as well as detecting early skin cancers [36,37]. In general, the authors believe that this method has the feasibility to be utilized for any biopsy tissue sample characterization for faster results. These computational results also need to be experimentally validated to support these remarks.

Conclusion

High-frequency ultrasound (22-41 MHz) analysis was conducted to identify the mitotic rate and nuclear pleomorphism level in breast tumor tissue in a finite element analysis study. Mitotic rate was mimicked by added malignant cells and pleiomorphism was mimicked by increasing nucleus size in the model geometry of breast tissue. Malignant cell density and nucleus size was varied at multiple levels for the ultrasound measurement. The circular and elliptical cellular shapes were used for both histological features. Ultrasound peak density and MPVD parameters were evaluated to detect the different combinations of malignant features. Peak density showed a strong increasing pattern against the in-

creasing number of malignant cells and malignant nucleus size for both cellular shapes. In contrast to that, the MPVD parameter responded with a decreasing trend against the histological features only for the circular cell shape. For the elliptical cell shape, MPVD failed to provide a conclusive trend. Among the two histological features, malignant cell density was found dominant against the response parameters. The spectral patterns were also evaluated for all malignant feature combinations. The jaggedness increased in the frequency spectrum with increasing feature levels. A large peak was observed at the center region (30-35 MHz) of the frequency range for the normal tissue and primary malignant tissue. The center peak disappeared with increasing nuclear pleomorphism. By studying the spectral pattern, pleomorphism information could potentially be extracted. Overall, spectral variation in the frequency level showed a distinguishable pattern with different tumor grades.

Funding

None

Ethical approval

Not required

Declaration of Competing Interest

None declared

CRediT authorship contribution statement

Koushik Paul: Conceptualization, Methodology, Software, Formal analysis, Data curation, Writing – original draft. **Jeremy Stromer:** Visualization, Data curation, Writing – review & editing. **Samuel Razmi:** Formal analysis, Investigation, Writing – review & editing. **Barbara A. Pockaj:** Supervision, Data curation, Writing – review & editing. **Leila Ladani:** Conceptualization, Resources, Writing – review & editing, Supervision, Project administration.

Reference

[1] Breast Cancer Diagnosis, Types of Breast Cancer n.d. https://www.cancer.org/cancer/breast-cancer/understanding-a-breast-cancer-diagnosis.html (accessed May 31, 2019).
[2] U.S. Breast Cancer Statistics | Breastcancer.org n.d. https://www.breastcancer.org/symptoms/understand_bc/statistics (accessed March 18, 2019).
[3] J Metzcar, Y Wang, R Heiland, P. Macklin, A Review of Cell-Based Computational Modeling in Cancer Biology, JCO Clin Cancer Informatics (2019) 1–13, doi:10.1200/cci.18.00069.
[4] K Atwell, SJ Dunn, JM Osborne, H Kugler, EJA. Hubbard, How computational models contribute to our understanding of the germ line, Mol Reprod Dev 83 (2016) 944–957, doi:10.1002/MRD.22735.
[5] G Maskarinec, IS Pagano, MA Little, SM Conroy, S-Y Park, LN. Kolonel, Mammographic density as a predictor of breast cancer survival: the Multiethnic Cohort, Breast Cancer Res 15 (2013) R7, doi:10.1186/bcr3378.
[6] P Crystal, SD Strano, S Shcharynski, MJ. Koretz, Using sonography to screen women with mammographically dense breasts, Am J Roentgenol 181 (2003) 177–182, doi:10.2214/ajr.181.1.1810177.
[7] BL Sprague, RE Gangnon, V Burt, A Trentham-Dietz, JM Hampton, RD Wellman, et al., Prevalence of mammographically dense breasts in the United States, J Natl Cancer Inst 106 (2014), doi:10.1093/jnci/dju255.
[8] C van Dooijeweert, PJ van Diest, SM Willems, CCHJ Kuijpers, E van der Wall, LIH Overbeek, et al., Significant inter- and intra-laboratory variation in grading of invasive breast cancer: A nationwide study of 33,043 patients in the Netherlands, Int J Cancer 146 (2020) 769–780, doi:10.1002/ijc.32330.
[9] K Rabe, OL Snir, V Bossuyt, M Harigopal, R Celli, ES. Reisenbichler, Interobserver variability in breast carcinoma grading results in prognostic stage differences, Hum Pathol 94 (2019) 51–57, doi:10.1016/j.humpath.2019.09.006.
[10] B Alacam, B Yazici, N Bilgutay, F Forsberg, C. Piccoli, Breast tissue characterization using FARMA modeling of ultrasonic RF echo, Ultrasound Med Biol 30 (2004) 1397–1407, doi:10.1016/J.ULTRASMEDBIO.2004.08.023.
[11] XZ Liu, XF Gong, D Zhang, SG Ye, B. Rui, Ultrasonic characterization of porcine liver tissue at frequency between 25 to 55 MHz, World J Gastroenterol 12 (2006) 2276–2279, doi:10.3748/wjg.v12.i14.2276.
[12] FL Lizzi, M Astor, EJ Feleppa, M Shao, A. Kalisz, Statistical framework for ultrasonic spectral parameter imaging, Ultrasound Med Biol 23 (1997) 1371–1382, doi:10.1016/S0301-5629(97)00200-7.
[13] ML Oelze, JF Zachary, WD O'brien, B. Program, Characterization of tissue microstructure using ultrasonic backscatter: Theory and technique for optimization using a Gaussian form factor, AsaScitationOrg 112 (2002) 1202–1211, doi:10.1121/1.1501278.
[14] TE. Doyle, Iterative simulation of elastic wave scattering in arbitrary dispersions of spherical particles, J Acoust Soc Am 119 (2006) 2599–2610, doi:10.1121/1.2184989.
[15] TE Doyle, AT Tew, KH Warnick, BL. Carruth, Simulation of elastic wave scattering in cells and tissues at the microscopic level, J Acoust Soc Am 125 (2009) 1751–1767, doi:10.1121/1.3075569.
[16] ML Oelze, JF. Zachary, Examination of cancer in mouse models using high-frequency quantitative ultrasound, Ultrasound Med Biol 32 (2006) 1639–1648, doi:10.1016/J.ULTRASMEDBIO.2006.05.006.
[17] Y Bige, Z Hanfeng, W. Rong, Analysis of microstructural alterations of normal and pathological breast tissue in vivo using the AR cepstrum, Ultrasonics 44 (2006) 211–215, doi:10.1016/J.ULTRAS.2005.11.001.
[18] K. Mercado, Developing high-frequency quantitative ultrasound techniques to characterize three-dimensional engineered tissues, University of Rochester; University of Rochester, Rochester, NY, USA, 2015.
[19] JD. Stromer, Evaluation of Soft Material Microstructure through High-frequency Ultrasound, Doctoral Dissertations, University of Connecticut, CT, USA, 2016.
[20] K Paul, L. Ladani, Relationship between peak density and acoustic scattering in high-frequency ultrasound wave propagation, SN Appl Sci 2 (2020) 1418, doi:10.1007/s42452-020-03208-w.
[21] FG. Mitri, Extrinsic extinction cross-section in the multiple acoustic scattering by fluid particles, J Appl Phys 121 (2017), doi:10.1063/1.4980117.
[22] K Paul, J Stromer, S Razmi, BA Pockaj, L Ladani, J. Razmi, Computational Modeling of Ultrasound C-Scan Imaging Using Transmitted Signal Peak Density, Appl Sci 11 (11) (2021) 4924 Page 4924 2021, doi:10.3390/APP11114924.
[23] A Aubry, A Derode, M. Tanter, Extraction of the multiple scattering contribution in weakly scattering media: Application to human soft tissues, J Acoust Soc Am 123 (2008) 3001–3001, doi:10.1121/1.2932568.
[24] K Paul, S Razmi, BA Pockaj, L Ladani, J. Stromer, Finite Element Modeling of Quantitative Ultrasound Analysis of the Surgical Margin of Breast Tumor, Tomogr 8 (8) (2022) 570–584 Pages 570-584 2022, doi:10.3390/TOMOGRAPHY8020047.
[25] J Stromer, L. Ladani, Influence of Microstructure on the High-Frequency Ultrasound Measurement of Peak Density, J Nondestruct Eval Diagnostics Progn Eng Syst 1 (2018), doi:10.1115/1.4041067.
[26] J Stromer, L. Ladani, Examination of a spectral-based ultrasonic analysis method for materials characterization and evaluation, Biomed Signal Process Control 40 (2018) 454–461, doi:10.1016/j.bspc.2017.10.010.
[27] H Schöndorf, H. Naujoks, Determining the nuclear area in normal breast epithelia and in the nucleic of mammary carcinomas, J Cancer Res Clin Oncol 1985 1093 109 (1985) 241–244, doi:10.1007/BF00390363.
[28] BD Lawrence, Z Pan, A Liu, DL Kaplan, MI. Rosenblatt, Human corneal limbal epithelial cell response to varying silk film geometric topography in vitro, Acta Biomater 8 (2012) 3732–3743, doi:10.1016/j.actbio.2012.06.009.
[29] M Yang, SL Baldwin, KR Marutyan, KD Wallace, MR Holland, JG. Miller, Elastic stiffness coefficients (c11, c33, and c13) for freshly excised and formalin-fixed myocardium from ultrasonic velocity measurements, J Acoust Soc Am 119 (2006) 1880–1887, doi:10.1121/1.2168547.
[30] RE Baddour, MD Sherar, JW Hunt, GJ Czarnota, MC. Kolios, High-frequency ultrasound scattering from microspheres and single cells, J Acoust Soc Am 117 (2005) 934–943, doi:10.1121/1.1830668.
[31] TE Doyle, RE Factor, CL Ellefson, KM Sorensen, BJ Ambrose, JB Goodrich, et al., High-frequency ultrasound for intraoperative margin assessments in breast conservation surgery: A feasibility study, BMC Cancer 11 (2011), doi:10.1186/1471-2407-11-444.
[32] RJ Gray, BA Pockaj, E Garvey, S. Blair, Intraoperative Margin Management in Breast-Conserving Surgery: A Systematic Review of the Literature, Ann Surg Oncol 25 (2018) 18–27, doi:10.1245/s10434-016-5756-4.
[33] MS Moran, SJ Schnitt, AE Giuliano, JR Harris, SA Khan, J Horton, et al., Society of Surgical Oncology-American Society for Radiation Oncology consensus guideline on margins for breast-conserving surgery with whole-breast irradiation in stages I and II invasive breast cancer, J Clin Oncol 32 (2014) 1507–1515, doi:10.1200/JCO.2013.53.3935.
[34] DQ Xue, C Qian, L Yang, XF. Wang, Risk factors for surgical site infections after breast surgery: A systematic review and meta-analysis, Eur J Surg Oncol 38 (2012) 375–381, doi:10.1016/j.ejso.2012.02.179.
[35] TP Olson, J Harter, A Muñoz, DM Mahvi, TM. Breslin, Frozen section analysis for intraoperative margin assessment during breast-conserving surgery results in low rates of re-excision and local recurrence, Ann Surg Oncol 14 (2007) 2953–2960, doi:10.1245/s10434-007-9437-1.
[36] EJ Feleppa, J Mamou, CR Porter, J. MacHi, Quantitative ultrasound in cancer imaging, Semin Oncol 38 (2011) 136–150, doi:10.1053/j.seminoncol.2010.11.006.
[37] J Levy, DL Barrett, N Harris, JJ Jeong, X Yang, SC Chen, High-frequency ultrasound in clinical dermatology: a review, Ultrasound J 13 (2021), doi:10.1186/s13089-021-00222-w.